Research Square

Preprints are preliminary reports that have not undergone peer review.
They should not be considered conclusive, used to inform clinical practice,
or referenced by the media as validated information.

Computational Study on the Adsorption of H2SiCl2 by Pristine, Al-, and Ga-Doped Boron Nitride Nanosheets: A DFT Study

Mohsen Doust Mohammadi
Tehran University: University of Tehran
hewa y abdullah (**hewayaseen@gmail.com**)
Tishk International University https://orcid.org/0000-0001-5766-3858

Research Article

Keywords: Boron Nitride nanosheet, Dichlorosilane, H2SiCl2, Natural bond orbital, NCI

Posted Date: February 23rd, 2021

DOI: https://doi.org/10.21203/rs.3.rs-220227/v1

License: This work is licensed under a Creative Commons Attribution 4.0 International License.
Read Full License

Computational study on the adsorption of H_2SiCl_2 by pristine, Al-, and Ga-doped boron nitride nanosheets: A DFT study

Mohsen Doust Mohammadi[a], Hewa Y. Abdullah[b,*]

[a] *School of Chemistry, College of Science, University of Tehran, Tehran 14176, Iran*

[b] *Physics Education Department, Faculty of Education, Tishk International University, 44001, Erbil, Iraq*

***corresponding author** Email: hewayaseen@gmail.com

Abstract

The density functional techniques (DFT) were put into practice to study the nature of the intermolecular interactions between Dichlorosilane (H_2SiCl_2) gas molecule with single-walled pristine, Al and Ga-doped boron nitride nanosheets (BNNS, BNAlNS, and BNGaNS, respectively). For performing optimization process, various functionals including PBE0, M06-2X, ωB97XD, and B3LYP-D3 were applied on both of the isolated and complex structures. All of the functionals were used together with split-valence triple-zeta basis sets with d-type Cartesian-Gaussian polarization functions (6-311G(d)). To consider the electronic structure, total density of state (DOS) analysis were employed. Natural bond orbital (NBO), quantum theory of atoms in molecules (QTAIM), and non-covalent interaction (NCI) analyses were also taken on board to discover the nature of intermolecular interactions between gas and nanosheets. The results of electronic structure calculations as well as population analyses has been carefully tabulated and partially depicted. The HOMO-LUMO energy gaps (HLG) were dramatically changed when the dopant atom added to the BNNS. It means the impurity can improve the sensivity and reactivity of the pristine nanosheet; therefore, by absorbing the H_2SiCl_2 onto the surface of the titled nanosheets, a salient signal can produce in a typical electronic circuit. Among all of the absorbents, BNGaNT shows the most favorable material to design a nanosensor for the studied gas molecule.

Keyword: Boron Nitride nanosheet; Dichlorosilane; H_2SiCl_2; Natural bond orbital; NCI.

1. Introduction

After the emergence of density functional theory (DFT) due to its high computational power for large molecules as well as its considerable accuracy and speed, a suitable framework was provided for the theoretical studies of chemical systems. Many scientists today use this method to understand the properties of chemical structures. Meanwhile, theoretical studies on nanoscale structures have found an extraordinary place in computational chemistry, and researchers have used numerous computational methods to study intermolecular interactions to design tools that have better accuracy and performance [1-5]. A variety of nanomaterials have been considered for the construction of sensors with high measurement accuracy, extreme insensitivity to temperature, very low response time, low production costs, and resistant to harsh environmental conditions [6-12].

Different of methods have been used in theoretical studies to improve the sensitivity of the adsorption process in nanomaterials such as metal doping [13-15], surface defect [16-18], transition metal decoration [19, 20], etc. Impurities introduced to the nanomaterial wall change the energy gap, and also dramatically change its morphology. Lin et al. provides a comprehensive study on the effect of transition metal decoration to boron nitride nanosheet [21]. Studies have shown that even the introduction of non-metals such as oxygen can activate the surface of nanomaterials [22]. Demonstrating the benefits of dopant element, we can point out that by reducing the electrical resistance, impurity-decorated nanomaterials can generate a stronger signal in the circuit. Therefore, compared to pure nanomaterials, it can be said that decorated nanomaterials have a higher efficiency [23]. Aluminum and gallium and germanium are the elements that have been widely used to activate the surface of nanosheets in theoretical studies [24-27].

BNNSs are easily synthesized by the chemical vapor deposition method [28]. Due to its remarkable mechanical, thermal, electrical and chemical properties, as well as its excellent reactivity and selectivity, BNNS is widely used [29-31]. The wide band gap (5-6 eV) classified BNNS as an electrical insulator [28, 32, 33]. Ahmadi et al. reported the values of energy gap and B-N bond length for BNNS 5.93 eV and 1.45 Å, respectively, and for Al-doped BNNS the band gaps as well as Al-N bond length are 5.39 eVand 1.74 Å, respectively [34]. BNNS is also a very successful nanosorbent and has been studied in many theoretical studies to detect H_2O [35] NO [36], CO [37], CH_2O [38], $COCl_2$ [39], C_2H_4 [40], and N_2O [41]. This nanosheet and metal decorated BNNS have also been used in the manufacture of many electronic devices [42-48]. It can also be used as a valuable material in the coating industry and metal protection because it is impermeable to gases and liquids and is also an electrical insulator [49-52].

This article encompasses a comprehensive study to investigate the intermolecular interactions of the H_2SiCl_2 gas molecule with pristine BNNS plus nanosheets doped with Al and Ga elements. The details information about the computational level was given in section 2. The result and discussion section has been divided in 4 separate subsections: Geometric Surveys (3.1.), which provides insights about bond length and other geometry properties as well as introducing the levels of study for optimizing all structures; Electronic Structure (3.2.) that discusses about DOS and energetic properties results; NBO analysis (3.3.) and QTAIM analysis (3.4) are provided to show the nature of intermolecular interactions between two fragments. We

tried to provide a brief theory for each part using useful references and avoided to bring boring description. And finally, the conclusion section briefly refers to all the findings in this study.

2. Computational details

All of the nanosheet structures were optimized using one-dimensional periodic boundary condition Kohn–Sham density functional theory [53-56] (PBC-DFT) method in vacuum. Various functionals such as PBE0 [57], M06-2X [58], ωB97XD [59], and B3LYP-D3 scheme of Grimme [60-62] together with split-valence triple-zeta basis sets with d-type Cartesian-Gaussian polarization functions (6-311G(d)) [63-71] were employed. There is no symmetry constraints were imposed. According to benchmark studies [72], such a basis set covers all we need in this study. A 3×3×1 k point sampling in the Brillouin zone integration [73] with kinetic energy cutoff of 450 eV was hired. In this approach, when the number of unit cells increase the total energy will become minimal. All the molecular geometries were built in Gaussview 6.0.16 [74] software package then fully optimized by the Berny [75] method by Gaussian 16 Rev. C.01 [76] linux based software. The optimization processes were performed using the default Gaussian convergence criteria. To configure the stability of each structure frequency calculation were done to determine the nature of the stationary points. In addition, the wave function stability calculations were also done to consider stability of the electrons. Natural bond orbital (NBO) calculations were carried out using the NBO v 3.1 software, which is integrated within Gaussian package to consider the charge-transfer interactions between occupied and unoccupied orbitals. To extract the result data of NBO, NCI, and QTAIM analyses, Multiwfn [77] software was used and GaussSum [78] package depicted the DOS diagrams.

The energy of adsorption (E_{ads}) between two fragments (nanosheet and H_2SiCl_2) can be considered as follows:

$$E_{ads} = E_{sheet/gas} - E_{sheet} - E_{gas} + \Delta E_{(BSSE)} \quad (1)$$

where $E_{sheet/gas}$ shows the total energy of the gas/nanosheet cluster. E_{sheet} and E_{gas} are the energies of the isolated nanosheet and isolated gas molecule, respectively. Basis set superposition error (BSSE) was obtained from the Boys and Bernardi's counterpoise procedure [79, 80] as follows:

$$\Delta E_{(BSSE)} = \Delta E_{cluster} - \Delta E_{sheet}^{cluster} - \Delta E_{gas}^{cluster} \quad (2)$$

According to Equation 1, negative values of E_{ads} (i.e. exothermic adsorptions) indicate that the formed complex is stable; otherwise, positive values of E_{ads} is belong to a local minimum in which the adsorption of H_2SiCl_2 and nansheet is detered by a energy barrier.

3. Results and discussion

3.1 Geometric Surveys

The PEB0 functional, hybrid form of Perdew–Burke–Ernzerhof (PBE) [81], together with 6-311G(d) basis set were selected at the first stage to start the geometry optimization process of the isolated and complex structures. Although PBE0 is fast, it cannot describe the long-range interactions, dispersion effect, and charge transfer excitations; therefore, all of the structures were re-optimized using robust methods like M06-2X, ωB97XD, and B3LYP-D3. Head-Gordon et al. [59] invented the ωB97XD functional to account for the effect of long-range interactions as well as the dispersion corrections. Among Minnesota 06 suit, which is developed by Truhlar et al. [82], the global hybrid functional with double non-local exchange (2X) amounts (i.e. M06-

2X) is a high performance method to study the non-covalent interactions. To study the dispersion effect, the latest version of B3LYP-D3 known as D3 (BD) (GD3BJ) developed by Grimme et al. [60-62] would be a good option. In order to compare the effect of each of the mentioned corrections, in Table 1, the amounts of adsorption energy obtained from PBE0 method can be evaluated with other more complex aforementioned methods.

The PBC-DFT framework at PBE0/6-311G(d) level was applied on a pristine $B_{18}N_{18}$ unit cell with 10.004 Å in each dimension. Figure 1 shows the selected boron nitride nanosheet (BNNS). Then the unit cell expanded 3 times along with each axis and the optimization process repeated with the same level of theory. It should be noted that, to reduce the boundary effects, the terminal atoms were terminated by H atoms. For the case for Al and Ga doped nanosheets, after the optimized expanded BNNS obtained, one of the boron atoms substituted by Al or Ga elements and calculations were performed at PBE0/6-311G(d) level of theory. The re-optimization processes were performed using 3 other functionals and same basis set. The values of bond length for BNNS, BNAlNS, and BNGaNS are depicted in Figure 2. As is obvious from Figure 2 (a), the B-N bond length is 1.45 Å. Also, Figures 2 (b) and (c) show the value of bond length for Al-N and Ga-N 1.71 Å and 1.74 Å , respectively. Due to the inner stress, the B-N bond length in the vicinity of Al ad Ga dopant atoms vary from 1.42 Å to 1.49 Å.

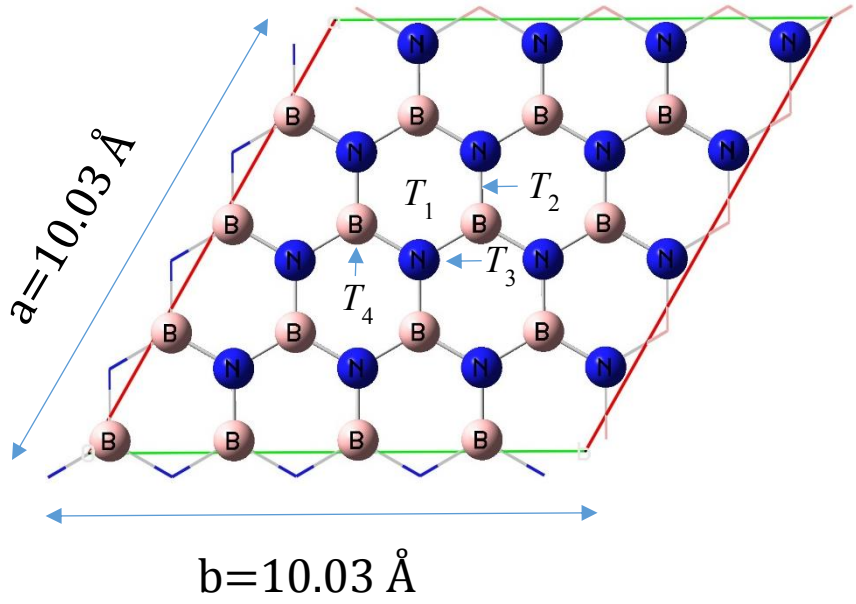

Figure 1. The unit cells for BNNS prepared to perform two-dimensional periodic boundary condition density functional theory calculations.

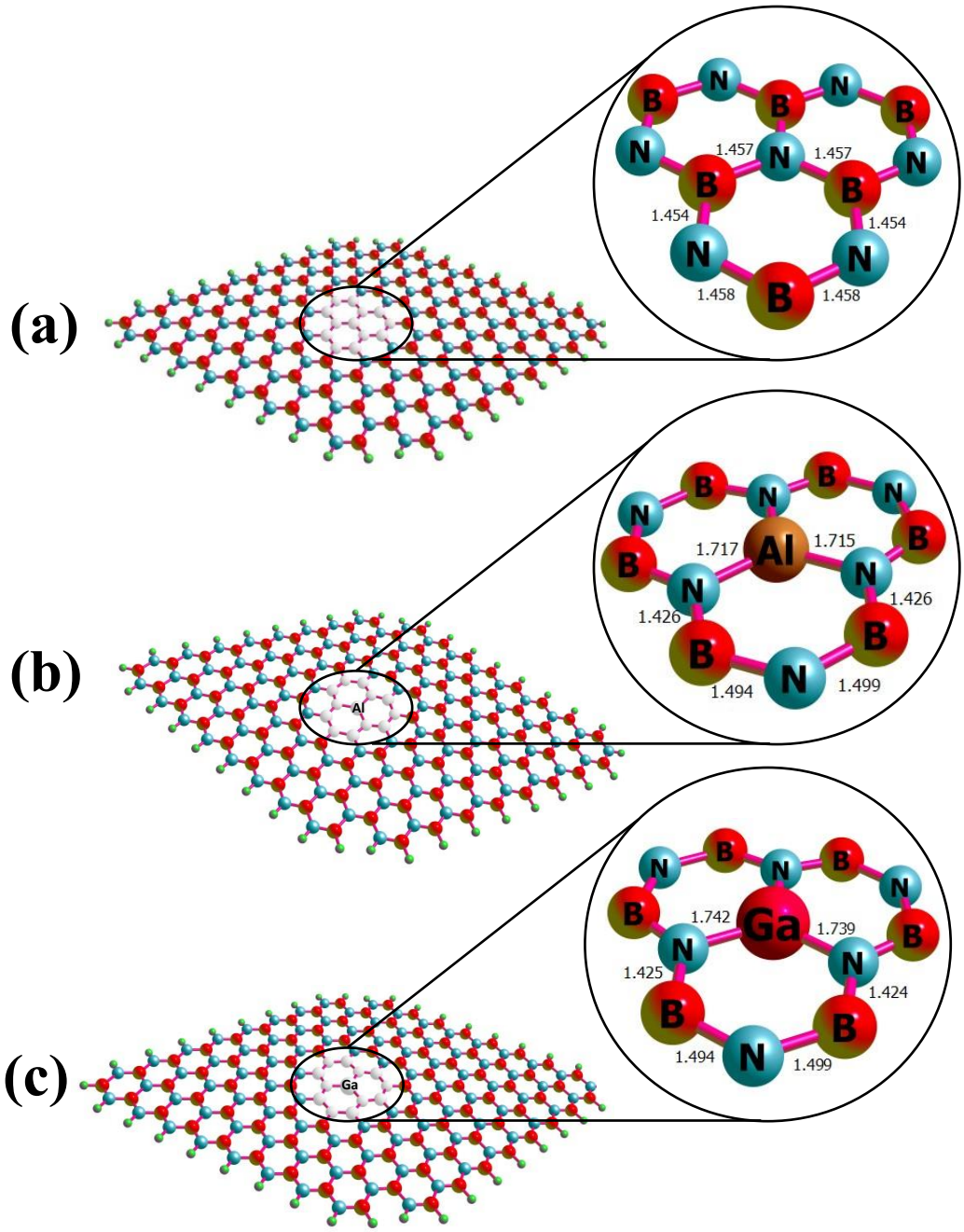

Figure 2. The bond length (Å) obtained at ωB97XD/6-311G(d) level for **(a)** BNNS, **(b)** BNAlNS, and **(c)** BNGaNS.

The adsorption of H_2SiCl_2 gas molecule onto the surface of pristine and Al, Ga-doped BNNS were also carried out. To achieve this goal, the gas molecule should be placed on top of the nanosheet in different positions through different orientations. The purpose of such calculations is to find energy local minima. Figure 3 shows the different heads of H_2SiCl_2

including H and Cl heads. There are 4 different sites in the BNNS (Figure 1) including: T_1, in the middle of hexagonal ring; T_2, between B and N atoms; T_3, N atom; and T_4, B atom. The gas molecule were put on top of each T_x sites through different distances and optimization process started at PM7/6-311G(d) level. It should be stressed that, overally, there are 80 initial orientations were prepared (i.e. 2×4×10=80. It means 6 different gas molecule heads were put on each of the 4 sites of nanosheet from 0.5 to 5.0 Å vertical distances with 0.5 Å intervals). Right after that, 4 minima were predicted. We select these 4 complex structures to optimize using PBE0/6-311G(d) level of theory. Regarding the values of adsorption energies , finally, the most stable complexes were chosen and re-optimization were done using other functionals including M06-2X, ωB97XD, and B3LYP-D3. The relaxed structures of all complexes which has been obtained from ωB97XD /6-311G(d) are depicted in Figure 4. When the values of E_{ads} are "below the range of chemical interest" [83], such results provides identical results.

The adsorption energy obtained from ωB97XD and B3LYP-D3 are closed to each other. The B3LYP-D3 functional shows the most negative E_{ads} values according to Table 1. It seems these two functional are good options for further investigations in this study. The most negative value of E_{ads} is corresponds to the adsorption of gas onto the Ga-doped BNNS, -1.176 eV which indicates that the reactivity of H_2SiCl_2 gas is significant. Otherwise, the reactivity of gas and pristine BNNS shows the weakest interaction, among those sheets. We preferred to run the population analysis calculations with ωB97XD to reduce the computation times. Therefore, all the interactions analyses were applied to the results of the ωB97XD /6-311G(d) level of theory.

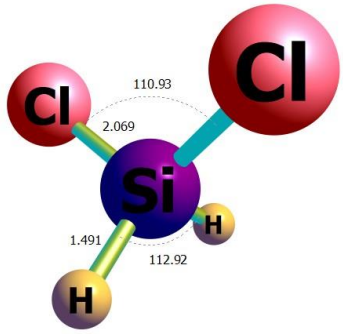

Figure 3. The relaxed structure of the H_2SiCl_2 gas molecule obtained from ωB97XD/6-311G(d) level of theory.

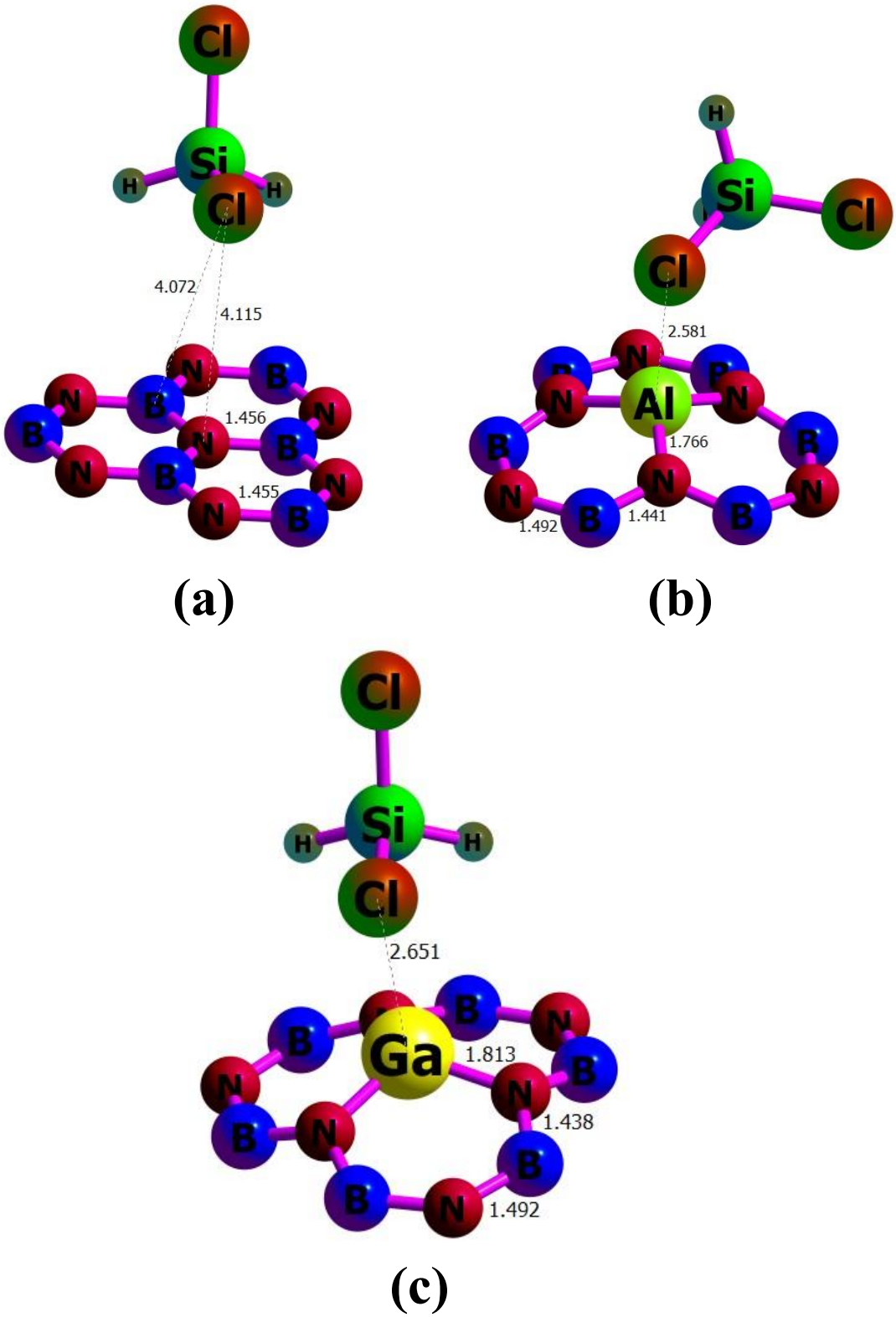

Figure 4. The relaxed structures of a) H_2SiCl_2/BNNS, b) H_2SiCl_2/BNAlNS, and c) H_2SiCl_2/BNGaNS obtained from ωB97XD/6-311G(d) level of theory.

Table1 The adsorption energies (E_{ads}) for H_2SiCl_2/nanosheet complexes. All values are in eV and obtained from geometry optimization calculations using PBE0, M06-2X, ωB97XD, and B3LYP-D3 functional in combination with 6-311G(d) basis set.

Systems	PBE0	M06-2X	wB97XD	B3LYP-D3
H_2SiCl_2/BNNS	-0.096	-0.205	-0.352	-0.393
H_2SiCl_2/BNAlNS	-0.691	-0.886	-0.985	-1.076
H_2SiCl_2/BNGaNS	-0.746	-1.116	-1.060	-1.176

3.2 Electronic Structure

The "Conceptual DFT" has been developed to consider the reactivity concept. Various properties can be obtained from HOMO-LUMO enrgy gap (HLG) [84] in such a way when an external potential apply to a system the energy, in the Hohenberg−Kohn theorems [56] context, changes as follows:

$$\begin{aligned}\Delta E &\equiv E\ N+\Delta N, v(\mathbf{r})+\Delta v(\mathbf{r})\ -E\ N, v(\mathbf{r})\\ &=\left(\frac{\partial E}{\partial N}\right)_v \Delta N+\int\left(\frac{\delta E}{\delta v(\mathbf{r})}\right)_N \delta v(\mathbf{r}) d(\mathbf{r})+\\ &\frac{1}{2!}\left\{\left(\frac{\partial^2 E}{\partial N^2}\right)_v \Delta N^2+2\int\left(\frac{\partial}{\partial N}\left(\frac{\delta E}{\partial v(\mathbf{r})}\right)_N\right)_v \Delta N\delta v(\mathbf{r})+\int\int\left(\frac{\partial^2 E}{\partial v^2(\mathbf{r})}\right)_N \delta v(\mathbf{r})\delta v(\mathbf{r}')d\mathbf{r}d\mathbf{r}'\right\}+\ldots\end{aligned} \quad (3)$$

In the above Taylor expansion N is a global quantity and $v(\mathbf{r})$ is a local function. Each term has a specifict meaning in the chemical language as follows:

$$-\chi=\left(\frac{\partial E}{\partial N}\right)_v=\mu\cong\frac{(\varepsilon_{LUMO}+\varepsilon_{HOMO})}{2} \quad (4)$$

$$\eta=\left(\frac{\partial \mu}{\partial N}\right)=\frac{1}{2}\left(\frac{\partial^2 E}{\partial N^2}\right)_v=\frac{1}{2}\ IP-EA \quad (5)$$

$$\omega=\frac{\mu^2}{2\eta} \quad (6)$$

Equation 4 shows the nagative electronegativity (χ) which is equal to chemical potential (μ). Also the values of HOMO and LUMO are related to the ionization affinity and electron affinity, respectively. You can follow the other terms to reach to the Fukui function, response function, dual descriptor, etc through literature [85, 86]. And Equation 6 is related to the electrophilicity index (ω). The values of these properties are listed in Table 2.

The energy gap (E_g) of BNNS has calculated about 5.729 eV at ωB97XD/6-311G (d) level of theory and the adsorption of H_2SiCl_2 on it reduced the energy gap to 5.687 eV. The Al and Ga-doped nanosheets were also reduced the E_g values. Table 2 Shows the LUMO values were

largely stabilized then the E_g has been reduced. The sensor response (S) is defined according to the following equations:

$$S = \left| \left(\frac{\sigma_1}{\sigma_2} \right) - 1 \right| = \exp\left(\frac{|\Delta E_g|}{kT} \right) - 1 \quad (7)$$

$$\sigma = AT^{3/2} e^{\frac{E_g}{2kT}} \quad (8)$$

Where A is a constant and σ is electrical conductivity, k is Boltzmann's constant, and T is Kelvin temperature. The resistivity will be diminished when E_g is being reduced, since the resistivity is proportional to the reciprocal of the conducting electron population. Hence, the resistivity for sheet/gas adsorption is low and the electric current generated in the circuit will face the lowest resistance. Density of state (DOS) map is useful in intuitively revealing density of distribution of molecular orbitals in different energy regions, and gap is directly visible from this map (Figure 5).

Table 2

HOMO energy (ε_H), LUMO energy (ε_L), Fermi energy (E_F), HOMO–LUMO energy gap (HLG), chemical potential (μ), chemical hardness (η), and electrophilicity (ω). All values are in eV and were obtained using the ωB97XD/6-311G(d) level of theory.

Systems	ε_H	ε_L	E_F	HLG	μ	η	ω
BNNS	-6.174	-0.446	-3.310	5.729	-3.310	2.864	15.692
BNAlNS	-6.177	-0.437	-3.307	5.739	-3.307	2.870	15.692
BNGaNS	-6.180	-0.438	-3.309	5.742	-3.309	2.871	15.716
H_2SiCl_2/BNNS	-6.217	-0.530	-3.373	5.687	-3.373	2.843	16.177
H_2SiCl_2/BNAlNS	-6.091	-1.423	-3.757	4.668	-3.757	2.334	16.474
H_2SiCl_2/BNGaNS	-6.204	-1.111	-3.657	5.092	-3.657	2.546	17.030

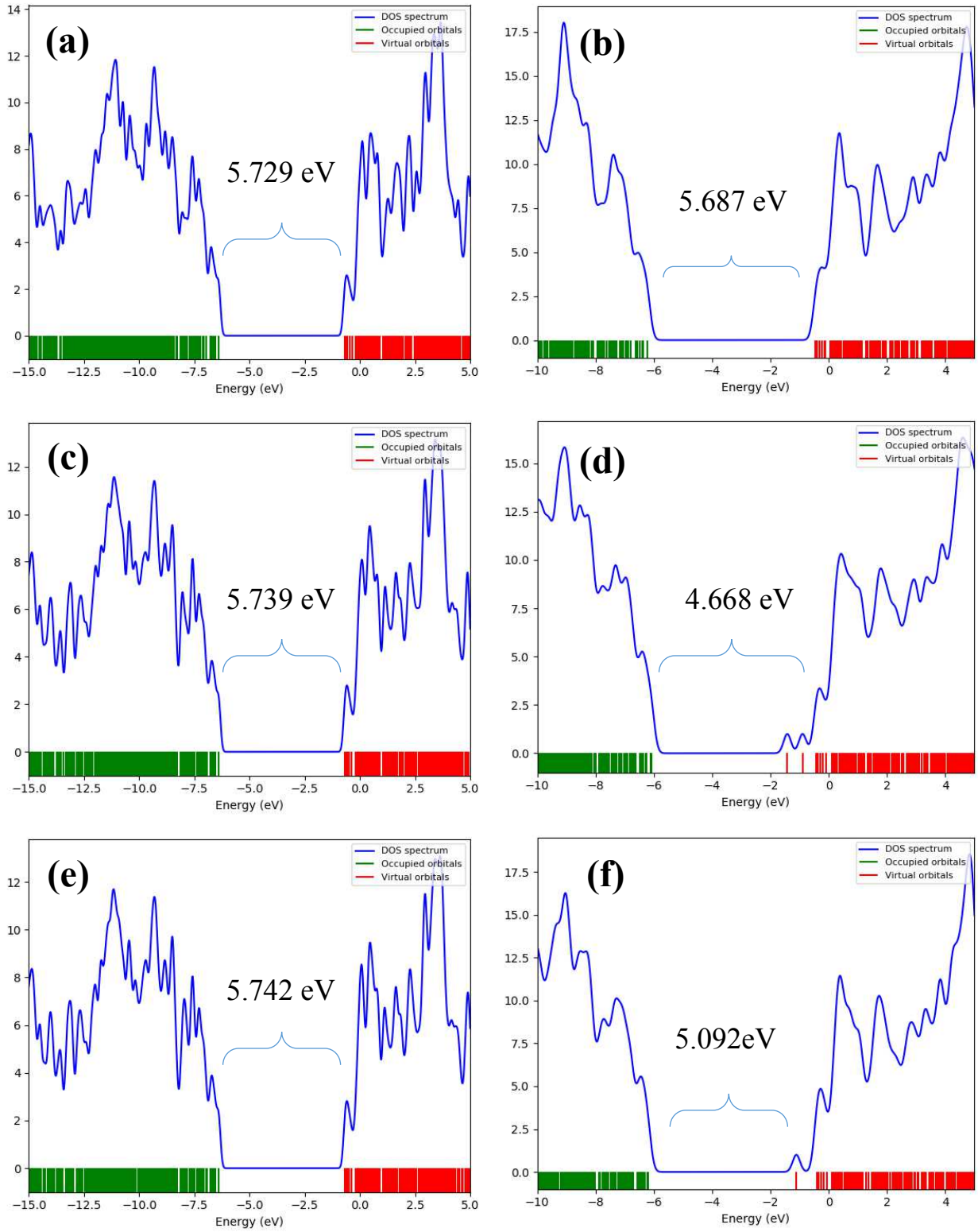

Figure 5. Density of state maps for (a) BNNS (b) H_2SiCl_2/BNNS (c) BNAlNS (d) H_2SiCl_2/BNAlNS (e) BNGaNS (f) H_2SiCl_2/BNGaNS. Data were obtained from the ωB97XD/6-311G(d) level of theory.

3.3 NBO Analysis

The Natural bond orbital (NBO) method, developed by Weinhold et al. [87-89], is one of the most respectful population analyses and uses to calculate the distribution of electron density in bonds between atoms. The term NBO refers to a bonding orbital with the maximum electron density. A density matrix, calculated from DFT, as well as atomic charge, are used to define natural bonding orbitals. To complete the span of valance space in addition to bonding NBO (σ), we need an antibonding NBO (σ*) as follows:

$$\sigma_{AB} = C_A h_A + C_B h_B \tag{9}$$

$$\sigma^*_{AB} = C_A h_A - C_B h_B \tag{10}$$

where h_A and h_B are natural hybrid valance orbitals, C_A and C_B are the corresponding polarization coefficients. In the present study, NBO calculations were performed to figure out various types of bond order including Mulliken [90] (Equation 11) and Mayer [91-93] (Equation 12) bond order as well as Wiberg bond index (WBI) in Löwdin orthogonalized basis [94, 95] (Equation 13). Thus,

$$I_{AB} = \sum_i \eta_i \sum_{a\in A}\sum_{b\in B} 2C_{a,i}C_{b,i}S_{a,b} = 2\sum_{a\in A}\sum_{b\in B} P_{a,b}S_{a,b} \tag{11}$$

$$I_{AB} = I^{\alpha}_{AB} + I^{\beta}_{AB} = 2\sum_{a\in A}\sum_{b\in B}\left[\ P^{\alpha}S_{\ ba}\ P^{\alpha}S_{\ ab} + P^{\beta}S_{\ ba}\ P^{\beta}S_{\ ab}\ \right] \tag{12}$$

$$I_{AB} = \sum_{a\in A}\sum_{b\in B} P^2_{ab} \tag{13}$$

In the above Equations, *P* and *S* are density and overlap matrix, respectively. Mulliken and Mayer's bond orders are sensitive to the basis set, spacially for the basis set including diffuse functions. On the other hand, Wiberg bond order with respect to the two other is less basis set dependence. Table 3 reports the values of obtained bond orders from different methods. According to the WBI which is more accurate than Mayer and Mulliken we can up to this conclusion that BNAlNS and BNGaNS adsorbents are more active material in this study for adsorbing H_2SiCl_2 rather than pristine BNNS. The bond order value shows that the interaction of the gas molcule with BNNS can be classified as physisorption; otherwise, the interactions between Al and Ge-doped BNNS with the gas are more strong van der Waals interactions.

Table 3 The values of Mulliken, Mayer, and Wiberg bond order obtained from the interactions of the CH_2N_2 molecule with BNNS, BNAlNS, and BNGaNS. All calculations were performed using the ωB97XD/6-311G(d) level of theory.

Systems	X.....Y	Mulliken	Mayer	Wiberg
H_2SiCl_2/BNNS	Cl.....B	0.083	0.122	0.88
H_2SiCl_2/BNAlNS	Cl.....Si	0.102	0.239	0.426
H_2SiCl_2/BNGaNS	Cl....Ge	0.168	0.296	0.549

(a) X atoms are belong to H_2SiCl_2

(b) Y atoms are belong to nanosheet

3.4 QTAIM Analysis

QTAIM analysis is used study bond types and intermolecular interactions. A critical point of the electron density, including minimum, maximum, or saddle point, can belong to: (1) *Atomic critical point* (ACP); (2) *bond critical point* (BCP); (3) *ring critical point* (RCP); and (4) *cage critical point* (CCP). The Electron density $\rho(\mathbf{r})$ and the Laplacian electron density $\nabla^2\rho(\mathbf{r})$ are playing important role in the QTAIM analysis since they determine the segmentation and identification of different types of chemical interactions. A bond critical point with negative values of Laplacian electron density and large values of electron density ($\rho(\mathbf{r})>10^{-1}$ a.u.) is defined as a covalent bond. On the other hand, the positive value of $\nabla^2\rho(\mathbf{r})$ designates that the interactions can be classified as of the non-substrate close-shell type (which include ionic and van der Waals interactions) [96].

The values of Lagrangian kinetic energy $G(\mathbf{r})$ and potential energy density $V(\mathbf{r})$ divulges the nature of the intermolecular interaction; therefore, the ratio of $G(\mathbf{r})/|V|(\mathbf{r})$ can be hired as an appropriate index in link classification. When $G(\mathbf{r})/|V|(\mathbf{r})$ <0.5, the nature of the interaction is covalent, and if $G(\mathbf{r})/|V|(\mathbf{r})$ >1, the interaction is non-covalent. For closed-shell interactions index at BCP is less than 1 and increases with increasing covalent character [97]. Large values of elliptical bond (ε) represent an unstable structure and defined as follows [98]:

$$\varepsilon = \frac{\lambda_1}{\lambda_2} - 1 \ , |\lambda_1| > |\lambda_2| \tag{14}$$

According to virial theorem [99], a relationship exists between $G(\mathbf{r})$, $V(\mathbf{r})$, and $\nabla^2\rho(\mathbf{r})$ as follows:

$$\frac{1}{4}\nabla^2\rho(\mathbf{r}) = 2G(\mathbf{r}) + V(\mathbf{r}) \tag{15}$$

From Table 4 all values for $\nabla^2\rho(\mathbf{r})$ are positive. The interactions between gas and BNNS show that the values of $G(\mathbf{r})/|V|(\mathbf{r})$ are higher than 1; therefore, for the case of BNNS and gas, the interactions are non-covalent. However, for doped BNNSs the values of $G(\mathbf{r})/|V|(\mathbf{r})$ are between 0.5 and 1. These results shows intermolecular interactions are classified as strong interactions. And finally the small values of ε and show that these structures are stable. Figure 6 are depicted to show the bond critical points between gas and nanosheets.

Table 4 QTAIM topological parameters for electron density (r), Laplacian of electron density ∇^2(r), kinetic electron density G(r), potential electron density V(r), bond ellipticity index (), and eta index ()at the BCPs of the CH_2N_2 clusters with BNNS, BNAlNS, and BNGaNS. All values were calculated using the ωB97XD/6-311G(d) level of theory and NBO analysis.

Systems	Bond		∇^2r	G(r)	V(r)	G(r)/V(r)		
H_2SiCl_2/BNNS	C.....N	0.004	0.013	0.002	-0.001	1.584	10.797	0.153
	C.....B	0.004	0.012	0.002	-0.002	1.301	4.006	0.122
	C.....N	0.004	0.011	0.002	-0.001	1.467	0.925	0.153
H_2SiCl_2/BNAlNS	Cl.....Al	0.023	0.066	0.019	-0.021	0.886	0.124	0.177
H_2SiCl_2/BNGaNS	Cl....Ga	0.031	0.086	0.025	-0.028	0.878	0.045	0.189
	C.....Ga	0.012	0.025	0.006	-0.007	0.974	0.344	0.129

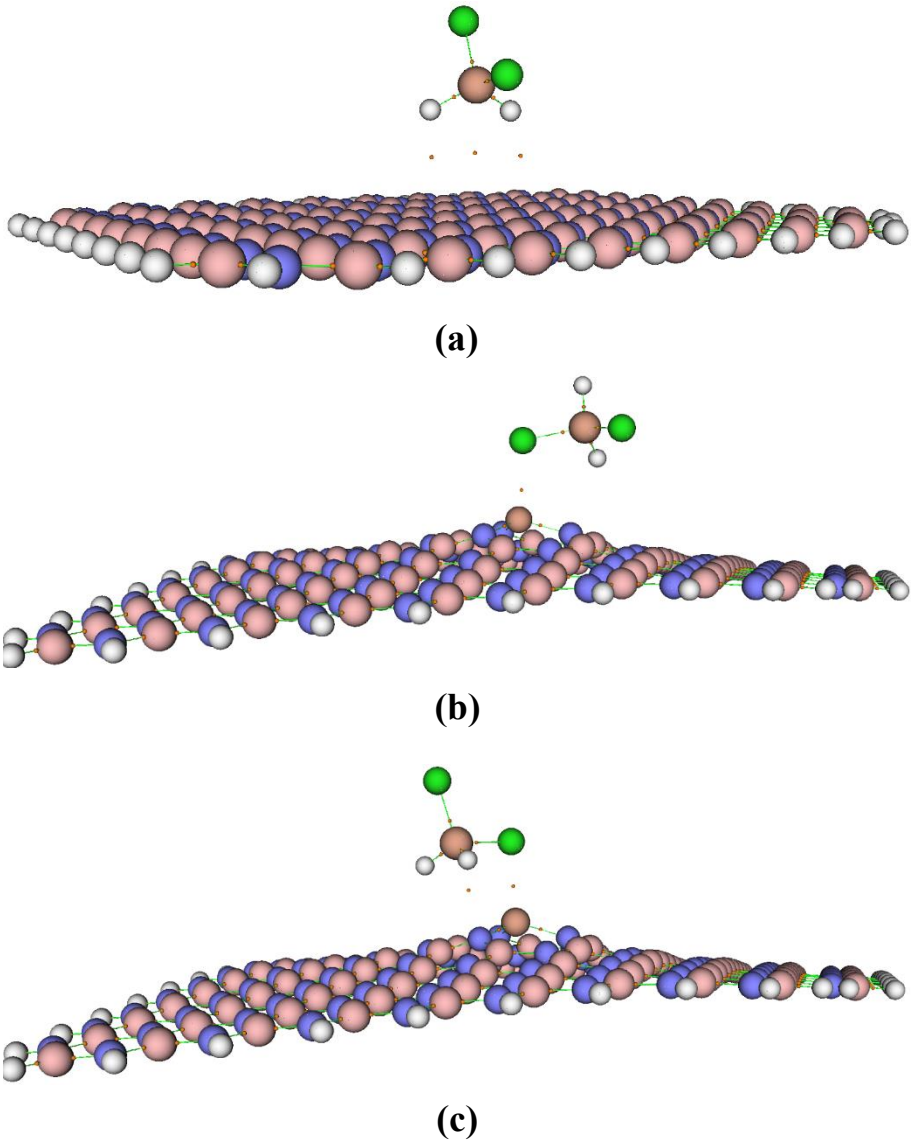

Figure 6. The Bond critical points graphs for (a) H_2SiCl_2/BNNS (b) H_2SiCl_2/BNAlNS (c) H_2SiCl_2/BNGaNS. Systems The orange dots represent the BCPs.

The results of QTAIM, in the previous section, showed that the interactions between H_2SiCl_2 and nanosheets are non-covalent; hence, it is useful to check them by a non-covalent analysis. Reduced density gradient (RDG) and sign$\lambda_2(r)\rho(r)$ are a pair of functions used in non-covalent interaction (NCI) [100] analysis which can be implemented to visualize the region and the type of weak interactions. RDG is defined as follows [100, 101]:

$$RDG = \frac{1}{2(3\pi^2)^{\frac{1}{3}}} \frac{\left|\overline{\Delta\rho}(\mathbf{r})\right|}{\overline{\rho(\mathbf{r})}^{\frac{4}{3}}} \quad (16)$$

The two functions RDG and sign$\lambda_2(\mathbf{r})\rho(\mathbf{r})$ can be plotted to define specific areas. In this case, non-covalent interactions will be identified. The points that indicate strong interactions are located in the sign$\lambda_2(\mathbf{r})\rho(\mathbf{r}) < 0$ region. Relatively weak van der Waals interactions are found in the sign$\lambda_2(\mathbf{r})\rho(\mathbf{r}) \approx 0$ region. And if points are in sign$\lambda_2(\mathbf{r})\rho(\mathbf{r}) > 0$ region, it means that the interactions are of the type of repulsive [100, 101]. As it turns out, bond strength is closely related to the density matrix $\rho(\mathbf{r})$ as well as signλ_2. Low RDG and low electron density regions should be consulted to determine whether non-covalent interactions occur between the two components involved in the adsorption process.

Considering an isosurface (Figure 7) as a reference (e.g. RDG = 0.5), it can be seen that the spots are appeared in the sign$\lambda_2(r)\rho(r) \approx 0$ zone after the adsorption of gas molecule onto BNNS; therefore, the interactions can classified as van der Waals. However, the interactions of gas with BNAlNS and BNGaNS were more stronger than BNNS in nature. NCI analysis also confirms the results of the adsorption energy calculations, QTAIM analysis, and NBO analysis, namely that the interactions of H_2SiCl_2 with the doped nanosheets were strong

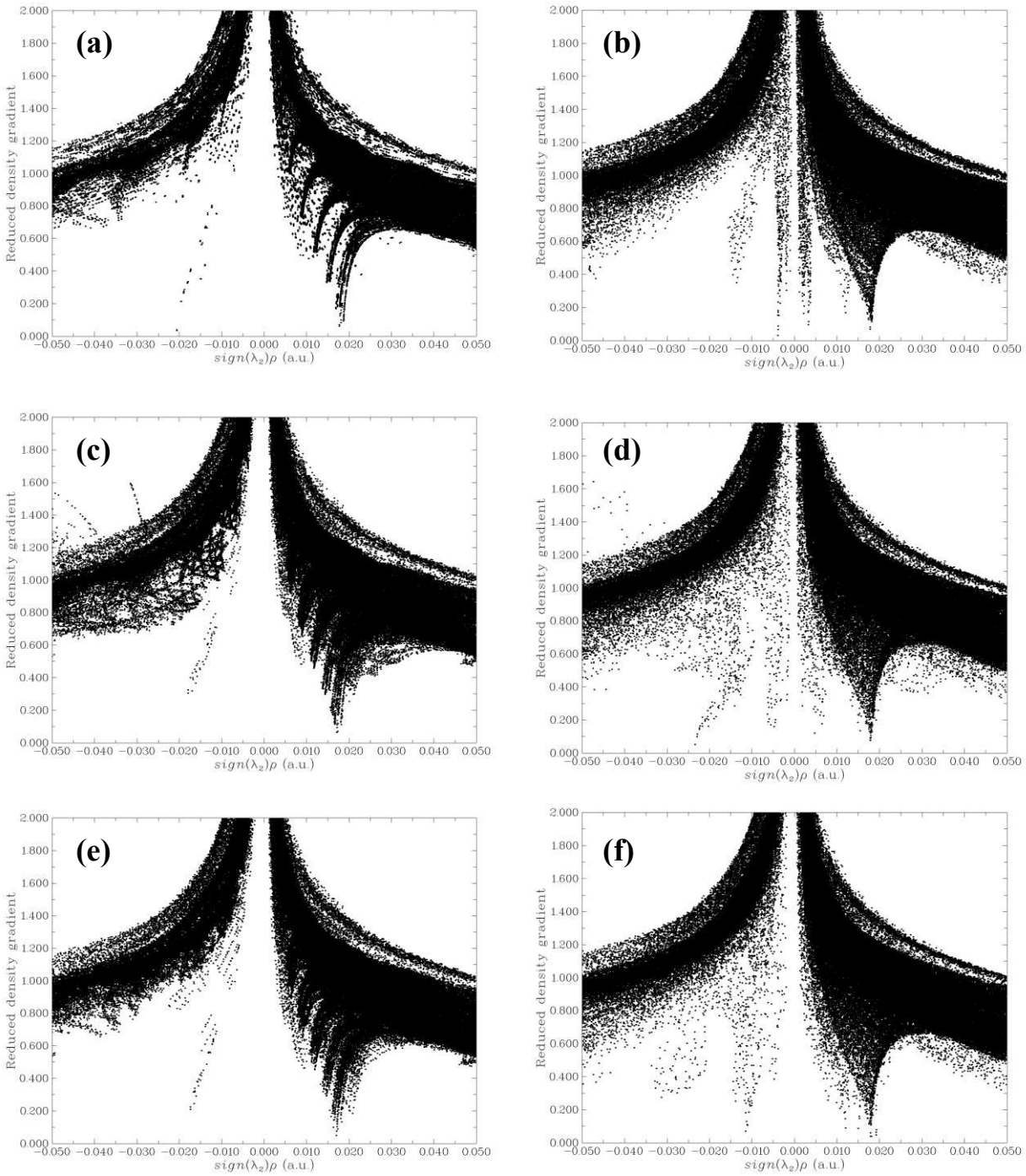

Figure 7. The RDG (X-axis) vs. sign(λ_2)ρ(r) (Y-axis) diagrams (a) BNNS (b) H_2SiCl_2/BNNS (c) BNAlNS (d) H_2SiCl_2/BNAlNS (e) BNGaNS (f) H_2SiCl_2/BNGaNS. The diagrams were obtained from ωB97XD/6-311G(d) level of theory.

4. Conclusion

The intermolecular interactions between the H_2SiCl_2 gas molecule and BNNS, BNAlNS, and BNGaNS were studied by the DFT framework in vacuum condition. All molecular structures optimized at PBE0, ωB97XD, M06-2X, and B3LYP-D3 functionals together wit a 6-311G(d) basis set. Relaxed structures obtained from ωB97XD/6-311G(d) were chosen for population analysis calculations. Results of adsorption energy show that among the nanosheets, the interaction of BNGaNT and gas (about -1.176 eV) is higher than the other adsorbents. Different bond order analysis data repeats former results. To shed light on the nature of intermolecular interactions NBO, QTAIM, and NCI analyses were implemented and the results of all the analyses were in agreement. From NBO analysis, the charge transfer was not observed and NCI and QTAIM results show van der Waals intermolecular interactions-specially for BNGaNS/gas cluster. To sum up, we can conclude injecting Al and Ga elements inside the BNNS can active its surface in favor of adsorbing H_2SiCl_2 gas. Accordingly, this nanomaterial would be favorable for designing a sensitive nanosensor.

Acknowledgements

I would like to thank the Solid-State Theory Group at the Physics Department at the Universita‘ degli Studi di Milano-Italy for providing computational facilities.

Declaration

Funding (information that explains whether and by whom the research was supported)

The authors declare that they have no known competing financial interests or personal relationships that could have appeared to influence the work reported in this paper.

Conflicts of interest/Competing interests (include appropriate disclosures)

The authors declare no conflict of interest

Availability of data and material (data transparency)

No data transparency available in manuscript

Code availability (software application or custom code)

Gaussian 16

Authors' contributions (optional: please review the submission guidelines from the journal whether statements are mandatory)

Mohsen Doust Mohammadi: Investigation, Writing - original draft. Hewa Y. Abdullah: Conceptualization, Writing - review & editing, Resources, Supervision.

Additional declarations for articles in life science journals that report the results of studies involving humans and/or animals

Not applicable

Ethics approval (include appropriate approvals or waivers)

Not applicable

Consent to participate (include appropriate statements)

Not applicable

Consent for publication (include appropriate statements)

Not applicable

References

[1] M. Kamel, A. Morsali, H. Raissi, K. Mohammadifard, Theoretical insights into the intermolecular and mechanisms of covalent interaction of Flutamide drug with COOH and COCl functionalized carbon nanotubes: a DFT approach, Chemical Review and Letters, 3 (2020) 23-37.

[2] R. Dos Santos, R. Rivelino, F. de Brito Mota, G. Gueorguiev, A. Kakanakova-Georgieva, Dopant species with Al–Si and N–Si bonding in the MOCVD of AlN implementing trimethylaluminum, ammonia and silane, Journal of Physics D: Applied Physics, 48 (2015) 295104.

[3] H. Ghafur Rauf, S. Majedi, E. Abdulkareem Mahmood, M. Sofi, Adsorption behavior of the Al-and Ga-doped B12N12 nanocages on COn (n= 1, 2) and HnX (n= 2, 3 and X= O, N): A comparative study, Chemical Review and Letters, 2 (2019) 140-150.

[4] F. Li, H. Asadi, DFT study of the effect of platinum on the H2 gas sensing performance of ZnO nanotube: explaining the experimental observations, Journal of Molecular Liquids, (2020) 113139.

[5] M.D. Mohammadi, M. Hamzehloo, The adsorption of bromomethane onto the exterior surface of aluminum nitride, boron nitride, carbon, and silicon carbide nanotubes: A PBC-DFT, NBO, and QTAIM study, Computational and Theoretical Chemistry, 1144 (2018) 26-37.

[6] M.D. Mohammadi, H.Y. Abdullah, The adsorption of chlorofluoromethane on pristine, and Al-and Ga-doped boron nitride nanosheets: a DFT, NBO, and QTAIM study, Journal of Molecular Modeling, 26 (2020) 1-15.

[7] M.D. Mohammadi, H.Y. Abdullah, Theoretical study of the adsorption of amantadine on pristine, Al-, Ga-, P-, and As-doped boron nitride nanosheets: a PBC-DFT, NBO, and QTAIM study, Theoretical Chemistry Accounts, 139 (2020) 1-17.

[8] M.D. Mohammadi, H.Y. Abdullah, The adsorption of bromochlorodifluoromethane on pristine and Ge-doped silicon carbide nanotube: a PBC-DFT, NBO, and QTAIM study, Structural Chemistry, (2020) 1-14.

[9] M.D. Mohammadi, I.H. Salih, H.Y. Abdullah, An Ultimate Investigation on the Adsorption of Amantadine on Pristine and Decorated Fullerenes C59X (X= Si, Ge, B, Al, Ga, N, P, and As): A DFT, NBO, and QTAIM Study, Journal of Theoretical and Computational Chemistry, (2020).

[10] E. Nemati-Kande, M. Abbasi, M. Doust Mohammadi, DFT, QTAIM and NBO Investigation of the Interaction of Rare Gases with Pristine and Decorated Boron Nitride Nanotube, ChemistrySelect, 3 (2018) 9833-9840.

[11] E. Nemati-Kande, M. Abbasi, M.D. Mohammadi, DFT studies on the interactions of pristine, Al and Ga-doped boron nitride nanosheets with CH3X (X= F, Cl and Br), Journal of Molecular Structure, 1199 (2020) 126962.

[12] E. Nemati-Kande, M. Abbasi, M.D. Mohammadi, Feasibility of Pristine and Decorated AlN and SiC Nanotubes in Sensing of Noble Gases: A DFT study, ChemistrySelect, 4 (2019) 2453-2462.
[13] K. Wilke, H. Breuer, The influence of transition metal doping on the physical and photocatalytic properties of titania, Journal of Photochemistry and Photobiology A: Chemistry, 121 (1999) 49-53.
[14] J.A. Botas, G. Calleja, M. Sánchez-Sánchez, M.G. Orcajo, Cobalt doping of the MOF-5 framework and its effect on gas-adsorption properties, Langmuir, 26 (2010) 5300-5303.
[15] D. Saha, S. Deng, Hydrogen adsorption on ordered mesoporous carbons doped with Pd, Pt, Ni, and Ru, Langmuir, 25 (2009) 12550-12560.
[16] K. Bolton, A QM/MM study of HCl adsorption at ice surface defect sites, Journal of Molecular Structure: THEOCHEM, 632 (2003) 145-156.
[17] L.-Q. Wang, D.R. Baer, M.H. Engelhard, A.N. Shultz, The adsorption of liquid and vapor water on TiO2 (110) surfaces: the role of defects, Surface science, 344 (1995) 237-250.
[18] Z. Wu, M. Li, J. Howe, H.M. Meyer III, S.H. Overbury, Probing defect sites on CeO2 nanocrystals with well-defined surface planes by Raman spectroscopy and O2 adsorption, Langmuir, 26 (2010) 16595-16606.
[19] K. Srinivasu, S.K. Ghosh, Transition metal decorated porphyrin-like porous fullerene: promising materials for molecular hydrogen adsorption, The Journal of Physical Chemistry C, 116 (2012) 25184-25189.
[20] T. Yildirim, J. Íñiguez, S. Ciraci, Molecular and dissociative adsorption of multiple hydrogen molecules on transition metal decorated C 60, Physical Review B, 72 (2005) 153403.
[21] S. Lin, X. Ye, R.S. Johnson, H. Guo, First-principles investigations of metal (Cu, Ag, Au, Pt, Rh, Pd, Fe, Co, and Ir) doped hexagonal boron nitride nanosheets: stability and catalysis of CO oxidation, The Journal of Physical Chemistry C, 117 (2013) 17319-17326.
[22] W. Lei, H. Zhang, Y. Wu, B. Zhang, D. Liu, S. Qin, Z. Liu, L. Liu, Y. Ma, Y. Chen, Oxygen-doped boron nitride nanosheets with excellent performance in hydrogen storage, Nano Energy, 6 (2014) 219-224.
[23] M. Hjiri, L. El Mir, S. Leonardi, A. Pistone, L. Mavilia, G. Neri, Al-doped ZnO for highly sensitive CO gas sensors, Sensors and Actuators B: Chemical, 196 (2014) 413-420.
[24] A.A. Darwish, M.M. Fadlallah, A. Badawi, A.A. Maarouf, Adsorption of sugars on Al-and Ga-doped boron nitride surfaces: A computational study, Applied Surface Science, 377 (2016) 9-16.
[25] M.D. Esrafili, S. Asadollahi, A comparative DFT study on single-atom catalysis of CO oxidation over Al-and P-embedded hexagonal boron-nitride nanosheets, Journal of Molecular Graphics and Modelling, 85 (2018) 323-330.
[26] A. Seif, K. Azizi, Charge-controlled switchable methane adsorption on heteroatom-doped BNNSs, RSC advances, 6 (2016) 5079-5088.
[27] A. Seif, K. Azizi, A new strategy for hydrogen storage using BNNS: simultaneous effects of doping and charge modulation, RSC advances, 6 (2016) 58458-58468.
[28] Y. Lin, J.W. Connell, Advances in 2D boron nitride nanostructures: nanosheets, nanoribbons, nanomeshes, and hybrids with graphene, Nanoscale, 4 (2012) 6908-6939.
[29] V. Guerra, C. Wan, T. McNally, Thermal conductivity of 2D nano-structured boron nitride (BN) and its composites with polymers, Progress in Materials Science, 100 (2019) 170-186.
[30] J.-l. Li, J.-h. Yin, T. Ji, Y. Feng, Y.-y. Liu, H. Zhao, Y.-p. Li, C.-c. Zhu, D. Yue, B. Su, Microstructure evolution effect on high-temperature thermal conductivity of LDPE/BNNS investigated by in-situ SAXS, Materials Letters, 234 (2019) 74-78.
[31] X. Yang, Y. Guo, Y. Han, Y. Li, T. Ma, M. Chen, J. Kong, J. Zhu, J. Gu, Significant improvement of thermal conductivities for BNNS/PVA composite films via electrospinning followed by hot-pressing technology, Composites Part B: Engineering, 175 (2019) 107070.
[32] L.H. Li, Y. Chen, Atomically thin boron nitride: unique properties and applications, Advanced Functional Materials, 26 (2016) 2594-2608.

[33] A. Falin, Q. Cai, E.J. Santos, D. Scullion, D. Qian, R. Zhang, Z. Yang, S. Huang, K. Watanabe, T. Taniguchi, Mechanical properties of atomically thin boron nitride and the role of interlayer interactions, Nature communications, 8 (2017) 1-9.
[34] A.A. Peyghan, M. Noei, S. Yourdkhani, Al-doped graphene-like BN nanosheet as a sensor for para-nitrophenol: DFT study, Superlattices and Microstructures, 59 (2013) 115-122.
[35] R. Omidirad, K. Azizi, DFT study of charge-controlled mechanism of water molecule dissociation on vacancy defected boron nitride nanosheets, Journal of Molecular Graphics and Modelling, 93 (2019) 107448.
[36] M.D. Esrafili, N. Saeidi, Carbon-doped boron nitride nanosheet as a promising catalyst for N2O reduction by CO or SO2 molecule: a comparative DFT study, Applied Surface Science, 444 (2018) 584-589.
[37] M.D. Esrafili, NO reduction by CO molecule over Si-doped boron nitride nanosheet: a dispersion-corrected DFT study, Chemical Physics Letters, 695 (2018) 131-137.
[38] M.D. Esrafili, P. Mousavian, F.A. Rad, Adsorption of formamide over pristine and Al-doped boron nitride nanosheets: A dispersion-corrected DFT study, Journal of Molecular Graphics and Modelling, 82 (2018) 101-107.
[39] R. Moladoust, M.D. Esrafili, A. Hosseinian, I. Alkorta, E. Vessally, Adsorption sensitivity of pristine and Al-or Si-doped boron nitride nanoflake to COCl2: a DFT study, Molecular Physics, 117 (2019) 626-634.
[40] M.D. Esrafili, Epoxidation of ethylene over carbon and silicon-doped boron nitride sheets: A comparative DFT study, Solid State Communications, 284 (2018) 35-39.
[41] M.D. Esrafili, S. Asadollahi, S. Heydari, A DFT study on NO reduction to N2O using Al-and P-doped hexagonal boron nitride nanosheets, Journal of Molecular Graphics and Modelling, 89 (2019) 41-49.
[42] R.W. Dorn, M.J. Ryan, T.-H. Kim, T.W. Goh, A. Venkatesh, P.M. Heintz, L. Zhou, W. Huang, A.J. Rossini, Identifying the Molecular Edge Termination of Exfoliated Hexagonal Boron Nitride Nanosheets with Solid-State NMR Spectroscopy and Plane-Wave DFT Calculations, Chemistry of Materials, 32 (2020) 3109-3121.
[43] Z. Ai, B. Chang, C. Xu, B. Huang, Y. Wu, X. Hao, Y. Shao, Interface engineering in the BNNS@ Ti 3 C 2 intercalation structure for enhanced electrocatalytic hydrogen evolution, New Journal of Chemistry, 43 (2019) 8613-8619.
[44] J. Azamat, A. Khataee, S.W. Joo, Separation of copper and mercury as heavy metals from aqueous solution using functionalized boron nitride nanosheets: A theoretical study, Journal of Molecular Structure, 1108 (2016) 144-149.
[45] M.D. Esrafili, N. Saeidi, A DFT study on the healing of N-vacancy defects in boron nitride nanosheets and nanotubes by a methylene molecule, International Journal of Quantum Chemistry, 117 (2017) e25450.
[46] M.D. Esrafili, N. Saeidi, P. Nematollahi, The healing of B-or N-vacancy defective BNNTs by using CO molecule: a DFT study, New Journal of Chemistry, 40 (2016) 8024-8031.
[47] H. Li, Z. Chen, X. Fang, D. Tie, Absorption of NH3 on pristine and defected boron nitride nanosheets: A first principle study, Superlattices and Microstructures, 88 (2015) 371-376.
[48] S. Lin, J. Huang, X. Gao, A Cu (111) supported h-BN nanosheet: a potential low-cost and high-performance catalyst for CO oxidation, Physical Chemistry Chemical Physics, 17 (2015) 22097-22105.
[49] L.H. Li, T. Xing, Y. Chen, R. Jones, Boron nitride nanosheets for metal protection, Advanced materials interfaces, 1 (2014) 1300132.
[50] L. Fu, G. Chen, N. Jiang, J. Yu, C.-T. Lin, A. Yu, In situ growth of metal nanoparticles on boron nitride nanosheets as highly efficient catalysts, Journal of Materials Chemistry A, 4 (2016) 19107-19115.
[51] W. Luo, Y. Wang, E. Hitz, Y. Lin, B. Yang, L. Hu, Solution processed boron nitride nanosheets: synthesis, assemblies and emerging applications, Advanced Functional Materials, 27 (2017) 1701450.

[52] M.A. Raza, A. Nadeem, M.T. Ilyas, Corrosion Study of Boron Nitride Nanosheets Deposited on Copper Metal by Electrophoretic Deposition, TMS 2019 148th Annual Meeting & Exhibition Supplemental Proceedings, Springer, 2019, pp. 681-685.
[53] F.M. Bickelhaupt, E.J. Baerends, Kohn-Sham density functional theory: predicting and understanding chemistry, Reviews in computational chemistry, 15 (2000) 1-86.
[54] J.A. Pople, P.M. Gill, B.G. Johnson, Kohn—Sham density-functional theory within a finite basis set, Chemical physics letters, 199 (1992) 557-560.
[55] W. Kohn, L.J. Sham, Self-consistent equations including exchange and correlation effects, Physical review, 140 (1965) A1133.
[56] P. Hohenberg, W. Kohn, Inhomogeneous electron gas, Physical review, 136 (1964) B864.
[57] J.P. Perdew, M. Ernzerhof, K. Burke, Rationale for mixing exact exchange with density functional approximations, The Journal of chemical physics, 105 (1996) 9982-9985.
[58] Y. Zhao, D.G. Truhlar, The M06 suite of density functionals for main group thermochemistry, thermochemical kinetics, noncovalent interactions, excited states, and transition elements: two new functionals and systematic testing of four M06-class functionals and 12 other functionals, Theoretical Chemistry Accounts, 120 (2008) 215-241.
[59] J.-D. Chai, M. Head-Gordon, Long-range corrected hybrid density functionals with damped atom–atom dispersion corrections, Physical Chemistry Chemical Physics, 10 (2008) 6615-6620.
[60] S. Grimme, Semiempirical GGA-type density functional constructed with a long-range dispersion correction, Journal of computational chemistry, 27 (2006) 1787-1799.
[61] S. Grimme, J. Antony, S. Ehrlich, H. Krieg, A consistent and accurate ab initio parametrization of density functional dispersion correction (DFT-D) for the 94 elements H-Pu, The Journal of chemical physics, 132 (2010) 154104.
[62] S. Grimme, S. Ehrlich, L. Goerigk, Effect of the damping function in dispersion corrected density functional theory, Journal of computational chemistry, 32 (2011) 1456-1465.
[63] R. Binning Jr, L. Curtiss, Compact contracted basis sets for third-row atoms: Ga–Kr, Journal of Computational Chemistry, 11 (1990) 1206-1216.
[64] L.A. Curtiss, M.P. McGrath, J.P. Blaudeau, N.E. Davis, R.C. Binning Jr, L. Radom, Extension of Gaussian-2 theory to molecules containing third-row atoms Ga–Kr, The Journal of Chemical Physics, 103 (1995) 6104-6113.
[65] M.J. Frisch, J.A. Pople, J.S. Binkley, Self-consistent molecular orbital methods 25. Supplementary functions for Gaussian basis sets, The Journal of chemical physics, 80 (1984) 3265-3269.
[66] P.J. Hay, Gaussian basis sets for molecular calculations. The representation of 3 d orbitals in transition-metal atoms, The Journal of Chemical Physics, 66 (1977) 4377-4384.
[67] M.P.M. J.-P. Blaudeau, L. A. Curtiss, and L. Radom, Extension of Gaussian-2 (G2) theory to molecules containing third-row atoms K and Ca, J. Chem. Phys., 107 (1997) 5016-5021.
[68] J.S.B. K. Raghavachari, R. Seeger, and J. A. Pople, Self-Consistent Molecular Orbital Methods. 20. Basis set for correlated wave-functions, J. Chem. Phys., 72 (1980) 650-654.
[69] M.P. McGrath, L. Radom, Extension of Gaussian-1 (G1) theory to bromine-containing molecules, The Journal of chemical physics, 94 (1991) 511-516.
[70] K. Raghavachari, G.W. Trucks, Highly correlated systems. Excitation energies of first row transition metals Sc–Cu, The Journal of chemical physics, 91 (1989) 1062-1065.
[71] T.V. Russo, R.L. Martin, P.J. Hay, Density functional calculations on first-row transition metals, The Journal of chemical physics, 101 (1994) 7729-7737.
[72] L. Goerigk, S. Grimme, A thorough benchmark of density functional methods for general main group thermochemistry, kinetics, and noncovalent interactions, Physical Chemistry Chemical Physics, 13 (2011) 6670-6688.
[73] H. Ibach, H. Lüth, An Introduction to Principles of Materials Science, Solid State and Physics, Springer, Berlin, (1995) 244.
[74] R. Dennington, T.A. Keith, J.M. Millam, GaussView, version 6.0. 16, Semichem Inc. Shawnee Mission KS, (2016).

[75] J. Baker, An algorithm for geometry optimization without analytical gradients, Journal of computational chemistry, 8 (1987) 563-574.
[76] M.J. Frisch, G.W. Trucks, H.B. Schlegel, G.E. Scuseria, M.A. Robb, J.R. Cheeseman, G. Scalmani, V. Barone, G.A. Petersson, H. Nakatsuji, X. Li, M. Caricato, A.V. Marenich, J. Bloino, B.G. Janesko, R. Gomperts, B. Mennucci, H.P. Hratchian, J.V. Ortiz, A.F. Izmaylov, J.L. Sonnenberg, Williams, F. Ding, F. Lipparini, F. Egidi, J. Goings, B. Peng, A. Petrone, T. Henderson, D. Ranasinghe, V.G. Zakrzewski, J. Gao, N. Rega, G. Zheng, W. Liang, M. Hada, M. Ehara, K. Toyota, R. Fukuda, J. Hasegawa, M. Ishida, T. Nakajima, Y. Honda, O. Kitao, H. Nakai, T. Vreven, K. Throssell, J.A. Montgomery Jr., J.E. Peralta, F. Ogliaro, M.J. Bearpark, J.J. Heyd, E.N. Brothers, K.N. Kudin, V.N. Staroverov, T.A. Keith, R. Kobayashi, J. Normand, K. Raghavachari, A.P. Rendell, J.C. Burant, S.S. Iyengar, J. Tomasi, M. Cossi, J.M. Millam, M. Klene, C. Adamo, R. Cammi, J.W. Ochterski, R.L. Martin, K. Morokuma, O. Farkas, J.B. Foresman, D.J. Fox, Gaussian 16 Rev. C.01, Wallingford, CT, 2016.
[77] T. Lu, F. Chen, Multiwfn: a multifunctional wavefunction analyzer, Journal of computational chemistry, 33 (2012) 580-592.
[78] N.M. O'boyle, A.L. Tenderholt, K.M. Langner, Cclib: a library for package-independent computational chemistry algorithms, Journal of computational chemistry, 29 (2008) 839-845.
[79] S.F. Boys, F. Bernardi, The calculation of small molecular interactions by the differences of separate total energies. Some procedures with reduced errors, Molecular Physics, 19 (1970) 553-566.
[80] I. Alkorta, C. Trujillo, J. Elguero, M. Solimannejad, A theoretical study of the hydrogen bonding properties of H2BNH2: Some considerations on the basis set superposition error issue, Computational and Theoretical Chemistry, 967 (2011) 147-151.
[81] J.P. Perdew, K. Burke, M. Ernzerhof, Generalized gradient approximation made simple, Physical review letters, 77 (1996) 3865.
[82] F. Ma, Z.-R. Li, Z.-J. Zhou, D. Wu, Y. Li, Y.-F. Wang, Z.-S. Li, Modulated nonlinear optical responses and charge transfer transition in endohedral fullerene dimers Na@ C60C60@ F with n-fold covalent bond (n= 1, 2, 5, and 6) and long range ion bond, The Journal of Physical Chemistry C, 114 (2010) 11242-11247.
[83] J.B. Foresman, A. Frisch, Exploring chemistry with electronic structure methods: a guide to using Gaussian, (1996).
[84] J.-L. Bredas, Mind the gap!, Materials Horizons, 1 (2014) 17-19.
[85] P. Geerlings, F. De Proft, W. Langenaeker, Conceptual density functional theory, Chemical reviews, 103 (2003) 1793-1874.
[86] S.-B. Liu, Conceptual density functional theory and some recent developments, Acta Physico-Chimica Sinica, 25 (2009) 590-600.
[87] a.J. Foster, F. Weinhold, Natural hybrid orbitals, Journal of the American Chemical Society, 102 (1980) 7211-7218.
[88] F. Weinhold, C.R. Landis, Natural bond orbitals and extensions of localized bonding concepts, Chemistry Education Research and Practice, 2 (2001) 91-104.
[89] F. Weinhold, Discovering chemistry with natural bond orbitals, John Wiley & Sons2012.
[90] R.S. Mulliken, Electronic population analysis on LCAO–MO molecular wave functions. I, The Journal of Chemical Physics, 23 (1955) 1833-1840.
[91] I. Mayer, Charge, bond order and valence in the AB initio SCF theory, Chemical Physics Letters, 97 (1983) 270-274.
[92] I. Mayer, Improved definition of bond orders for correlated wave functions, Chemical Physics Letters, 544 (2012) 83-86.
[93] A.J. Bridgeman, G. Cavigliasso, L.R. Ireland, J. Rothery, The Mayer bond order as a tool in inorganic chemistry, Journal of the Chemical Society, Dalton Transactions, (2001) 2095-2108.
[94] K.B. Wiberg, Application of the pople-santry-segal CNDO method to the cyclopropylcarbinyl and cyclobutyl cation and to bicyclobutane, Tetrahedron, 24 (1968) 1083-1096.
[95] O.V. Sizova, L.V. Skripnikov, A.Y. Sokolov, Symmetry decomposition of quantum chemical bond orders, Journal of Molecular Structure: THEOCHEM, 870 (2008) 1-9.

[96] C.F. Matta, Hydrogen–Hydrogen Bonding: The Non-Electrostatic Limit of Closed-Shell Interaction Between Two Hydro, Hydrogen Bonding—New Insights, Springer2006, pp. 337-375.
[97] B. Niepötter, R. Herbst-Irmer, D. Kratzert, P.P. Samuel, K.C. Mondal, H.W. Roesky, P. Jerabek, G. Frenking, D. Stalke, Experimental charge density study of a silylone, Angewandte Chemie International Edition, 53 (2014) 2766-2770.
[98] H.J. Bohórquez, R.J. Boyd, C.F. Matta, Molecular model with quantum mechanical bonding information, The Journal of Physical Chemistry A, 115 (2011) 12991-12997.
[99] S.J. Grabowski, QTAIM characteristics of halogen bond and related interactions, The Journal of Physical Chemistry A, 116 (2012) 1838-1845.
[100] E.R. Johnson, S. Keinan, P. Mori-Sánchez, J. Contreras-García, A.J. Cohen, W. Yang, Revealing noncovalent interactions, Journal of the American Chemical Society, 132 (2010) 6498-6506.
[101] J. Contreras-García, E.R. Johnson, S. Keinan, R. Chaudret, J.-P. Piquemal, D.N. Beratan, W. Yang, NCIPLOT: a program for plotting noncovalent interaction regions, Journal of chemical theory and computation, 7 (2011) 625-632.

Figures

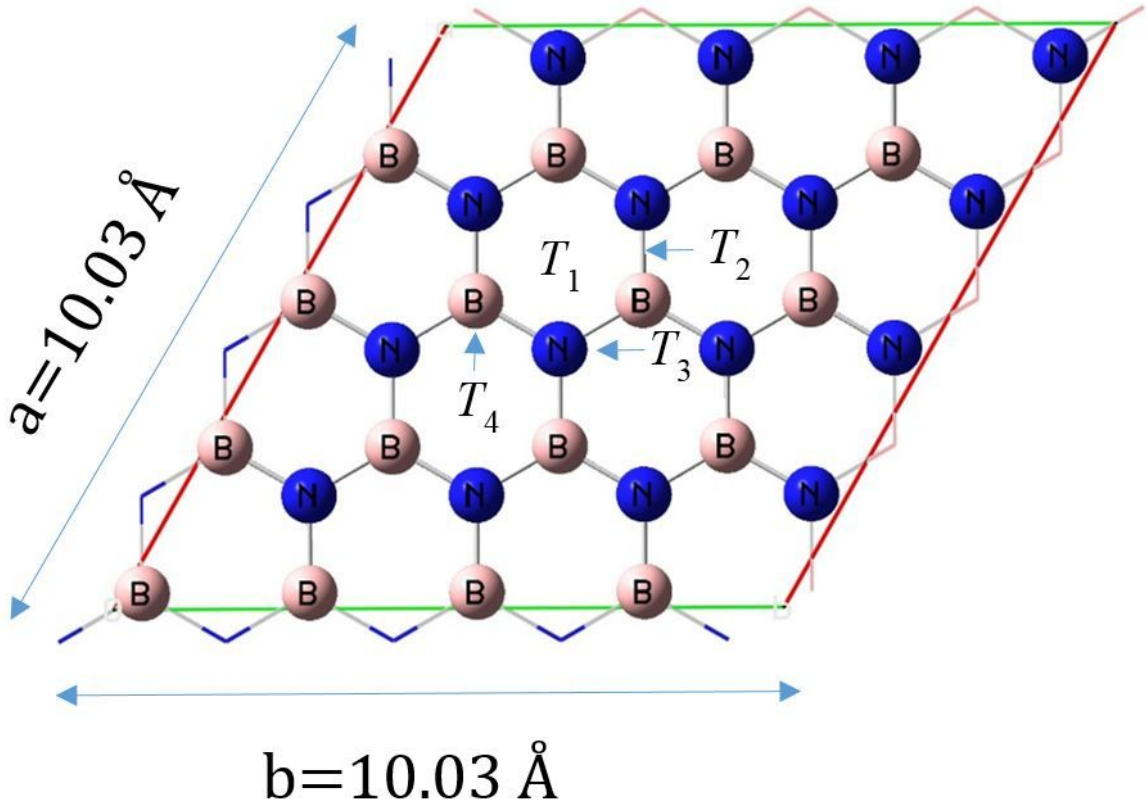

Figure 1

The unit cells for BNNS prepared to perform two-dimensional periodic boundary condition density functional theory calculations.

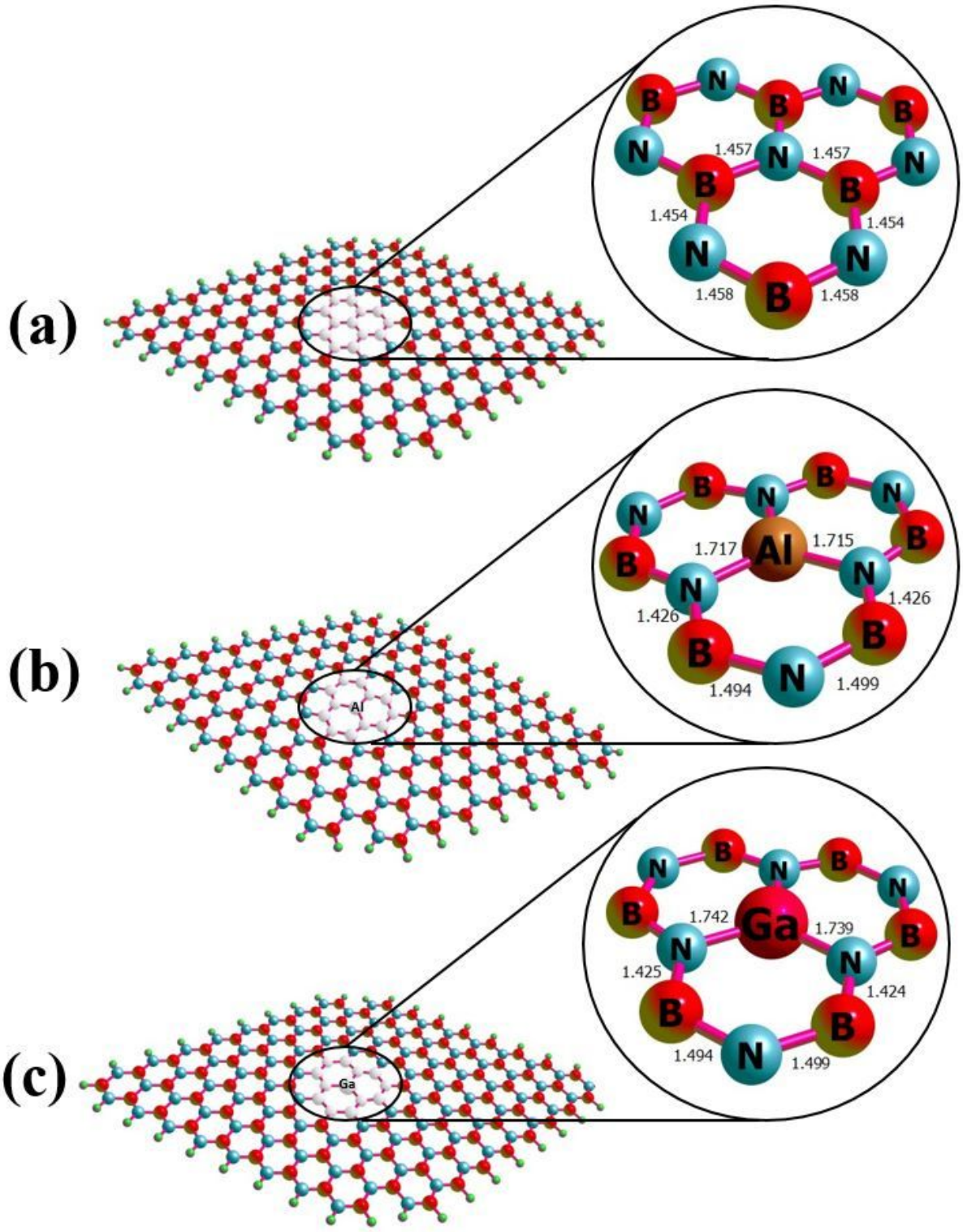

Figure 2

The bond length (Å) obtained at ωB97XD/6-311G(d) level for (a) BNNS, (b) BNAlNS, and (c) BNGaNS.

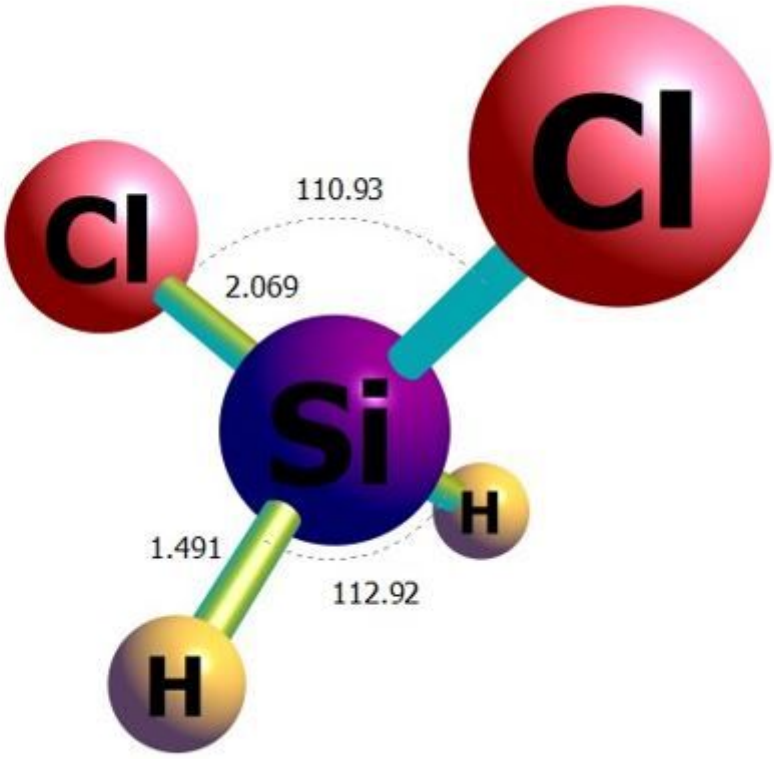

Figure 3

The relaxed structure of the H2SiCl2 gas molecule obtained from ωB97XD/6-311G(d) level of theory.

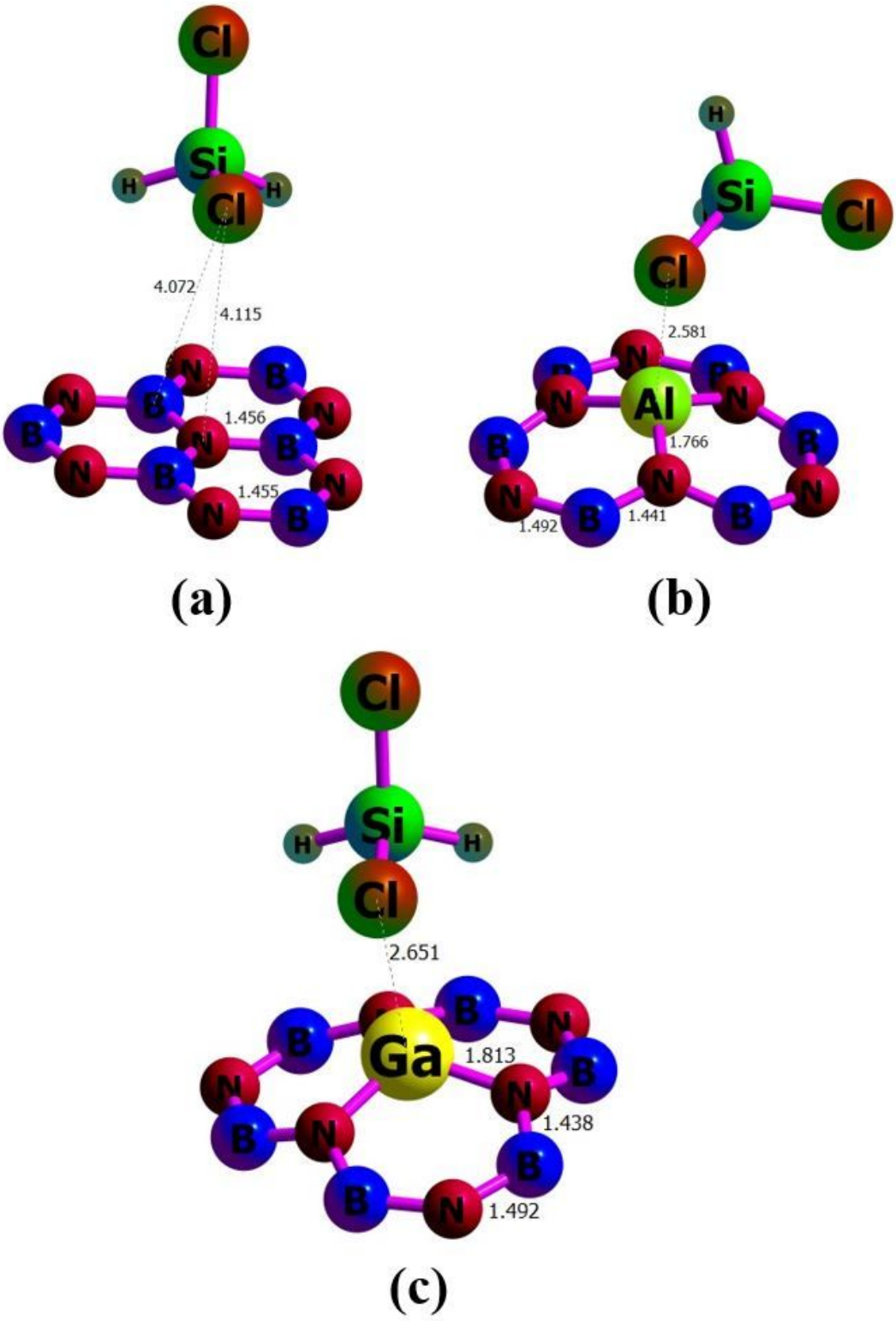

Figure 4

The relaxed structures of a) H2SiCl2/BNNS, b) H2SiCl2/BNAlNS, and c) H2SiCl2/BNGaNS obtained from ωB97XD/6-311G(d) level of theory.

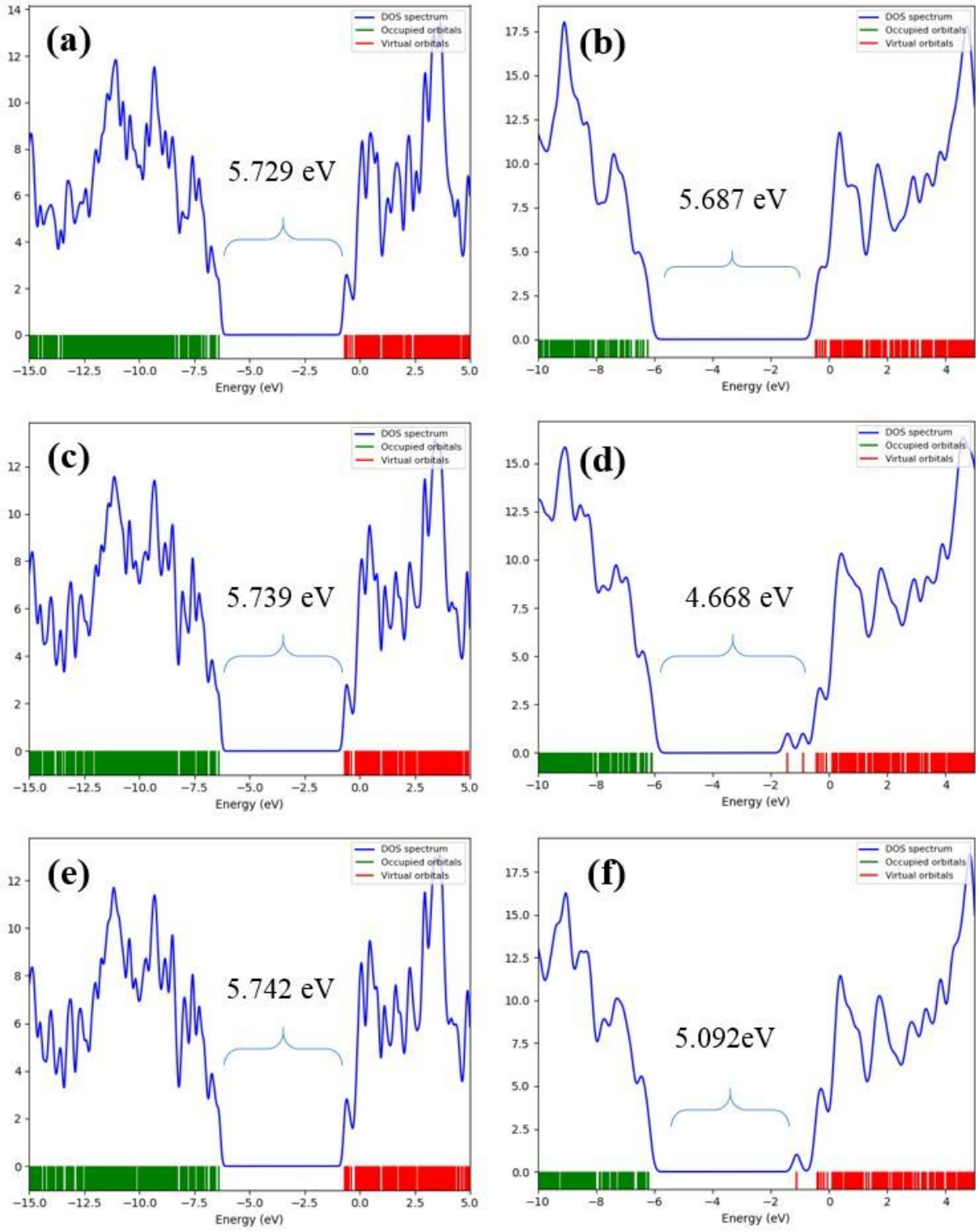

Figure 5

Density of state maps for (a) BNNS (b) H2SiCl2/BNNS (c) BNAlNS (d) H2SiCl2/BNAlNS (e) BNGaNS (f) H2SiCl2/BNGaNS. Data were obtained from the ωB97XD/6-311G(d) level of theory.

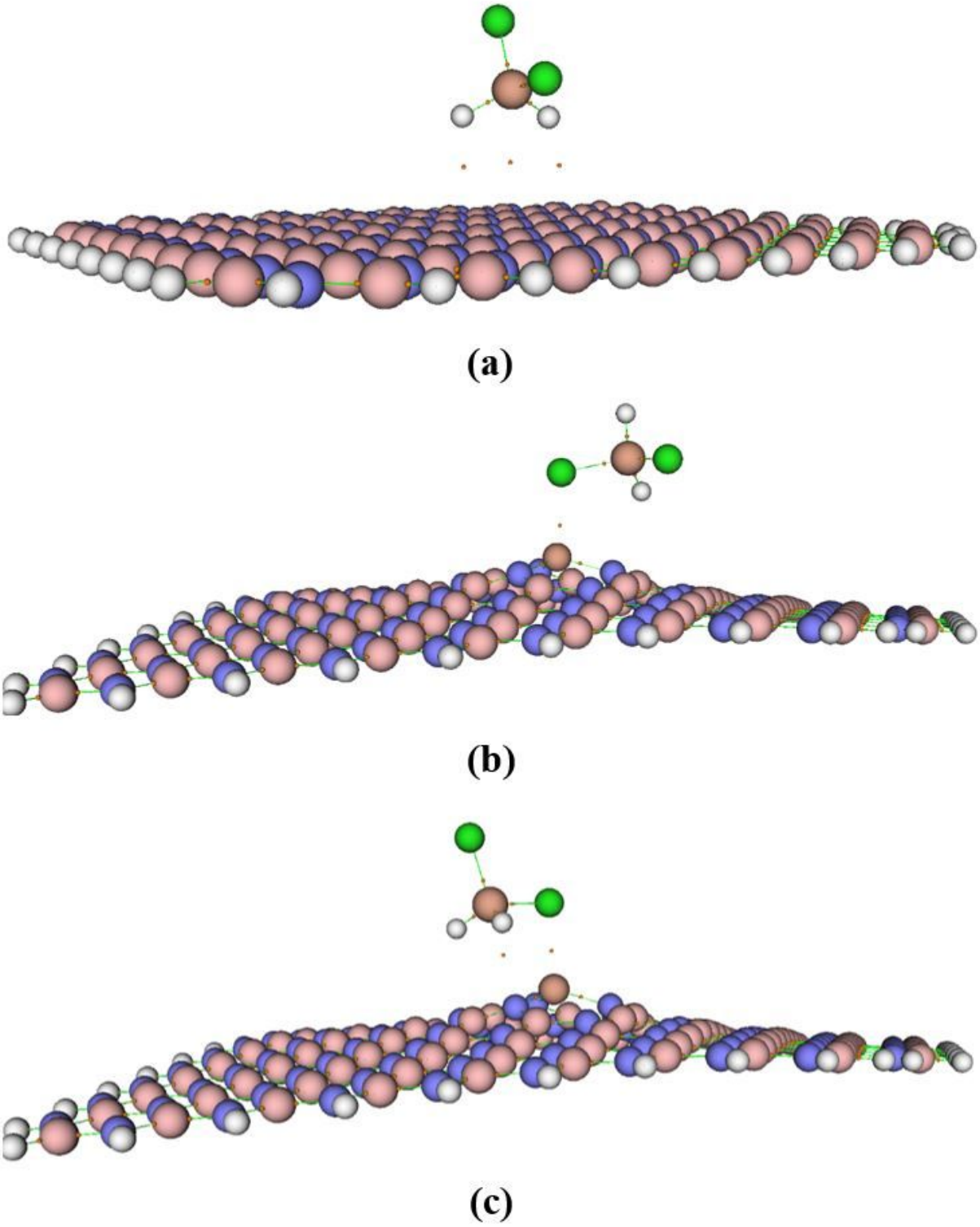

Figure 6

The Bond critical points graphs for (a) H2SiCl2/BNNS (b) H2SiCl2/BNAlNS (c) H2SiCl2/BNGaNS. Systems The orange dots represent the BCPs.

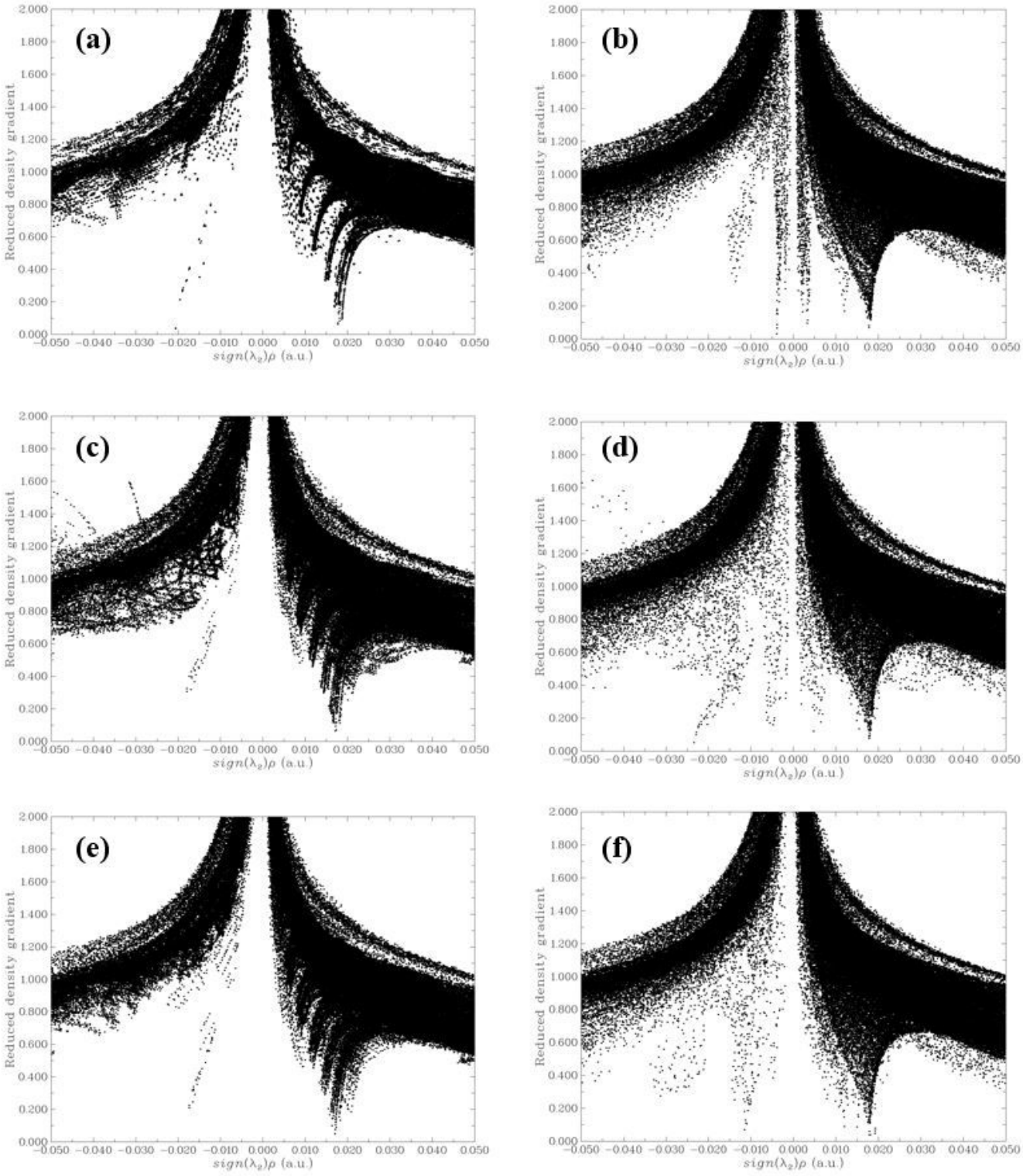

Figure 7

The RDG (X-axis) vs. sign(λ2)ρ(r) (Y-axis) diagrams (a) BNNS (b) H2SiCl2/BNNS (c) BNAlNS (d) H2SiCl2/BNAlNS (e) BNGaNS (f) H2SiCl2/BNGaNS. The diagrams were obtained from ωB97XD/6-311G(d) level of theory.